STRUCTURAL SCIENCE
CRYSTAL ENGINEERING
MATERIALS

ISSN: 2052-5206
journals.iucr.org/b

Crystal structures of two furazidin polymorphs revealed by a joint effort of crystal structure prediction and NMR crystallography

Marta K. Dudek, Piotr Paluch and Edyta Pindelska

Acta Cryst. (2020). B**76**, 322–335

Acta Cryst B STRUCTURAL SCIENCE CRYSTAL ENGINEERING MATERIALS

ISSN 2052-5206

Crystal structures of two furazidin polymorphs revealed by a joint effort of crystal structure prediction and NMR crystallography

Marta K. Dudek,[a]* Piotr Paluch[a] and Edyta Pindelska[b]*

[a]Center of Molecular and Macromolecular Studies, Polish Academy of Sciences, Sienkiewicza 112, Lodz, 90-363, Poland, and [b]Faculty of Pharmacy, Medical University of Warsaw, Banacha 1, Warsaw, 02097, Poland. *Correspondence e-mail: mdudek@cbmm.lodz.pl, edyta.pindelska@wum.edu.pl

Received 19 December 2019
Accepted 12 March 2020

Edited by A. Katrusiak, Adam Mickiewicz University, Poland

Keywords: polymorphism; NMR crystallography; crystal structure prediction; furazidin; crystal structure determination.

CCDC references: 1993854; 1993855

Supporting information: this article has supporting information at journals.iucr.org/b

This work presents the crystal structure determination of two elusive polymorphs of furazidin, an antibacterial agent, employing a combination of crystal structure prediction (CSP) calculations and an NMR crystallography approach. Two previously uncharacterized neat crystal forms, one of which has two symmetry-independent molecules (form I), whereas the other one is a $Z' = 1$ polymorph (form II), crystallize in $P2_1/c$ and $P\overline{1}$ space groups, respectively, and both are built by different conformers, displaying different intermolecular interactions. It is demonstrated that the usage of either CSP or NMR crystallography alone is insufficient to successfully elucidate the above-mentioned crystal structures, especially in the case of the $Z' = 2$ polymorph. In addition, cases of serendipitous agreement in terms of ^{1}H or ^{13}C NMR data obtained for the CSP-generated crystal structures different from the ones observed in the laboratory (false-positive matches) are analyzed and described. While for the majority of analyzed crystal structures the obtained agreement with the NMR experiment is indicative of some structural features in common with the experimental structure, the mentioned serendipity observed in exceptional cases points to the necessity of caution when using an NMR crystallography approach in crystal structure determination.

1. Introduction

Crystal structure prediction (CSP) of fairly rigid, small chemicals with one molecule in the asymmetric part of a unit cell has recently become an almost routine task (Price, 2018; Price *et al.*, 2016). This is mainly due to significant development of computational methods used in CSP in the last decades, leading to successful prediction of the most stable polymorphs of pharmaceutically relevant compounds (Bhardwaj *et al.*, 2019) and functional materials with desired properties (Pulido *et al.*, 2017), explanation of crystallization behavior and preferred supramolecular synthons formed in crystals of organic molecules (Dudek *et al.*, 2019), including formation of solvates and hydrates (Braun *et al.*, 2016; Dudek & Day, 2019; Braun *et al.*, 2019), enhancing our understanding of gelation performance of molecules (Piana *et al.*, 2016), as well as crystal structure determination of active pharmaceutical ingredients, for which attempts to obtain an appropriate crystal for single-crystal X-ray measurements have failed (Dudek *et al.*, 2018; Baias, Dumez *et al.*, 2013; Hofstetter *et al.*, 2019). Still, some challenges remain, including for example handling flexible molecules (Day *et al.*, 2007) and/or crystal structures with more than one molecule in the asymmetric part of a unit cell, as such CSP searches require significantly more degrees of freedom to be taken into account than the ones for $Z' = 1$ and rigid molecules (Price, 2014; Reilly *et al.*, 2016).

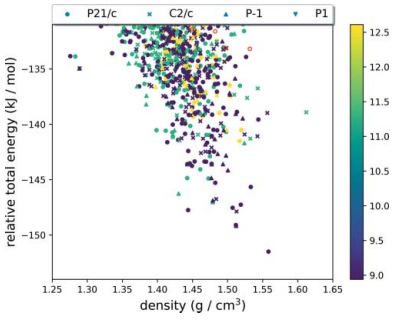

The above-mentioned challenges may be especially troublesome when using CSP as a method for crystal structure determination of polymorph(s) characterized before only by powder X-ray diffraction (PXRD), for which the crystal structure is difficult to solve with standard analytical techniques (single-crystal X-ray measurements, solution from PXRD diffractogram). Then, if a CSP search yields a structure which has noticeably lower energy than all other structures found in the same search, one may be fairly convinced that the searched polymorph has been found. Much more often, however, the number of structures found in the low-energy region of the crystal energy landscape obtained from a CSP search is significant, especially for $Z' > 1$ searches, for which there can be even several thousand crystal structures (Dudek *et al.*, 2016, 2017). This is still more problematic if we recall that the average error of state-of-the-art methods used for lattice energy minimization is *ca* 5–10 kJ mol^{-1}, a region in which one may often find tens of possible crystal structures. In such circumstances a comparison of all possible theoretical models with results from experimental methods (PXRD, solid-state NMR) is needed. On the other hand, these experimental methods can deliver structural constraints before any CSP search is attempted, thus considerably narrowing the number of degrees of freedom which should be accounted for. In this work we demonstrate such an approach to crystal structure determination of two previously uncharacterized polymorphs of furazidin (Fig. 1), an active pharmaceutical ingredient (API) used for the treatment of urinary tract infections.

As will be shown, one of the studied polymorphs of furazidin (form I) crystallizes with two molecules in the asymmetric part of a unit cell ($Z' = 2$), whereas the other one (form II) has only one symmetry-independent molecule, a feature which enabled us to compare the level of difficulty in crystal structure determination using a CSP–NMR approach between $Z' = 1$ and $Z' = 2$ polymorphs. This comparison includes the observed differences in extracting meaningful structural constraints from solid-state NMR and PXRD data, the number of crystal structures found in the low-energy region of the CSP crystal energy landscape, as well as the level of agreement with the experiment, especially in terms of NMR data. We also analyze cases of structures which display a very good agreement with the NMR experiment, despite being different from the actual experimental structure (false-positive indications).

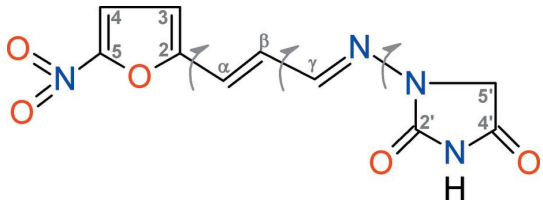

Figure 1
The chemical structure of furazidin with numbering of carbon atoms. Arrows indicate rotatable bonds included in the conformational search. The C5-NO_2 bond was kept rigid at its most energetically favourable position.

2. Materials and methods

2.1. Crystallization experiments

A powder sample of furazidin was obtained from Adamed Sp. z o. o., Czosnów, Poland. The phase purity of this polycrystalline sample was checked using PXRD and Fourier transform infrared spectroscopy (FT–IR) as compared with the published data (Liepins *et al.*, 2015). These measurements have shown that it was form I of furazidin. Additionally form II was prepared using previously published procedures (Liepins *et al.*, 2015). The newly obtained form II has also been studied for phase purity. The obtained patterns and spectra were consistent with the published ones (FT–IR spectra are given in Fig. S1 in the supporting information, while both PXRD data sets can be found in Fig. 3). The high-quality single crystals of the DMF (dimethylformamide) solvate monohydrate of furazidin were obtained by slow evaporation from DMF solution.

2.2. Solid-state NMR measurements

The majority of solid-state NMR measurements were performed with a Bruker Avance III 600 spectrometer, operating at 150.92 and 600.13 MHz for ^{13}C and ^{1}H, respectively. If not specified otherwise, samples were spun at 60 kHz using 1.3 mm Bruker ZrO_2 rotors. Chemical shifts were referenced with respect to finely powdered solid adamantane (1.8 p.p.m. for ^{1}H and 38.5 p.p.m. for ^{13}C). ^{1}H–^{13}C inverse-detected heteronuclear correlation (invHETCOR) experiments were performed with a pulse sequence described by Pruski and coworkers (Mao *et al.*, 2009; Althaus *et al.*, 2014). For both samples two experiments were measured with a different second contact time equal to 50 µs and 2000 µs, and first contact time was kept at the duration 2000 µs. In the first case (short second contact time of 50 µs) only C—H correlation through one bond is observed, while in the second case contacts between C and H nuclei located further apart in space (up to 4 Å) can also be observed. For ^{13}C cross-polarization magic-angle spinning (CP/MAS) and ^{1}H–^{13}C invHETCOR experiments a ramp-shaped pulse from 90 to 100% was applied on the proton channel during CP with precisely optimized RF (radiofrequency) field on ^{13}C, ^{15}N-labeled histidine hydrochloride) at around 160 kHz. On the ^{13}C channel an RF equal to 100 kHz during CP and $\pi/2$ pulses was applied. All experiments were performed with a low-power swept-frequency two-pulse phase modulation (SWf-TPPM) decoupling sequence (Chandran *et al.*, 2008) with an RF equal to 10 kHz. The repetition rate was set to 160 and 120 s for forms I and II, respectively. ^{1}H–^{1}H Back-to-Back correlation was measured with a spinning speed equal to 62.5 kHz, with a duration of excitation and reconversion periods of 32 µs. To increase resolution in the case of furazidin form I ^{1}H–^{13}C invHETCOR with a short second contact time was measured using a 800 MHz spectrometer with acquisition parameters exactly the same as before. This was done to ensure appropriate separation of the correlation peaks, resulting in an unambiguous and precise assignment of the ^{1}H resonances.

2.3. Powder X-ray diffraction experiments

Powder X-ray diffraction patterns were recorded at room temperature on a Bruker D8 Advance diffractometer equipped with a LYNXEYE position-sensitive detector using Cu $K\alpha$ radiation (λ = 0.15418 nm). The data were collected in Bragg–Brentano (θ/θ) horizontal geometry (flat reflection mode) between 3° and 45° (2θ) in a continuous scan using 0.03° steps and 384 s per step. The diffractometer incident beam path was equipped with a 2.5° Soller slit and a 1.14° fixed divergence slit, while the diffracted beam path was equipped with a programmable anti-scatter slit (fixed at 2.20°), a Ni β-filter and a 2.5° Soller slit. Data were collected under standard laboratory conditions.

Indexing of powder X-ray diffractograms was performed with the *Reflex* tool, as implemented in *Materials Studio* software, using *X-Cell* (Neumann, 2003) and searching through all possible crystal systems. Rietveld refinement was performed for the selected structures from a CSP search with *GSAS-II* software (Toby & Von Dreele, 2013), allowing cell parameters to be refined, while keeping atomic positions fixed.

2.4. FT–IR spectroscopy measurements

FT–IR studies were performed using a Perkin-Elmer Spectrum 1000 FT–IR spectrometer. Samples were mixed with KBr using a mortar and pestle to obtain a homogeneous mixture, then the powder was gently pressed under vacuum conditions with a compression force of 6.6 MPa using a 14 mm-diameter round flat force punch to produce a KBr pellet. Samples were placed in the light path and the IR spectra from 400 to 4000 cm^{-1}, resolution 2 cm^{-1}, in a transmission mode were registered. All spectra were prepared using *GRAMS* AI (version 8.0, Thermo Electron Corp., Waltham, MA, USA).

2.5. Differential scanning calorimetry (DSC) measurements

DSC measurements were performed on a differential scanning calorimeter DSC 2920, TA Instruments, in the temperature range of 273–573 K (0–300°C), with a heating rate of 2 K min^{-1}, nitrogen flow of 50 ml min^{-1}, and using aluminium pans. Temperature calibration was done in a two-point mode on indium and tin, and the data were acquired and analyzed with *Thermal Analyst* (TA Instruments, 1998) software. DSC results are available in the supporting information (Fig. S2).

2.6. Conformational search and CSP calculations

Conformational search has been performed using the *Conformers* tool as implemented in *Materials Studio* (Dassault Systèmes BIOVIA, 2016) software, using all three rotatable bonds with a 60° step for each bond. Subsequently all conformers have been optimized using universal force field, which yielded 22 different structures. Out of these, eight unique conformers were obtained after final optimization using *Gaussian16* software (Frisch *et al.*, 2016) and the B3LYP functional (Becke, 1993) supplemented by the Grimme D3 dispersion correction using Becke–Johnson damping (GD3BJ) (Grimme *et al.*, 2011) and the 6-311G(d,p) basis set.

For CSP calculations of the Z' = 1 polymorph (form II) four conformers selected on the basis of the NMR experiment were used. For each conformer, 10 000 successfully lattice-energy-minimized crystal structures were generated in each of the selected space groups, *i.e.* $P2_1/c$, $C2/c$, $P\overline{1}$ and $P1$. The space-group selection was made on the basis of indexing of the experimental powder X-ray diffractogram. Crystal structures were generated using *Global Lattice Energy Explorer* code (Case *et al.*, 2016) and the lattice energy minimized with *DMACRYS* 2.2.1.0 software (Price *et al.*, 2010), based on atom-centered distributed multipoles up to hexadecapoles, calculated for each conformer independently from B3LYP-D3BJ/6-311G** charge density using distributed multipole analysis (DMA) in *GDMA* 2.2.11 software (Stone, 2005). The electrostatic interactions were calculated as a sum of charge–charge, dipole–dipole and higher multipole interactions. Intermolecular interactions (repulsion–dispersion term) were calculated using FIT potential (Coombes *et al.*, 1996), with 25 Å cut-off on van der Waals interactions. To eliminate duplicates the obtained crystal structures were clustered on the basis of their energy and density (with a tolerance of 0.1 kJ mol^{-1} and 0.02 g cm^{-3}, respectively) and similarity of PXRD pattern. Final total energy for each structure is given as a sum of intra- and intermolecular energy contributions. The first term is the relative gas-phase energy of conformers with respect to the gas-phase global minimum, calculated at the B3LYP-D3BJ/6-311G** level of theory, whereas the second one is the lattice energy term obtained from *DMACRYS* lattice energy minimization.

CSP of the Z' = 2 polymorph of furazidin (form I) required a more extensive search than the one performed for form II. Therefore it was done in two stages. First 10 000 crystal structures were generated for each of 36 possible pairs of conformers in $P2_1$, Pc and $P\overline{1}$ space groups, using the same methodology as given above. Then, for the conformers that yielded the lowest-energy structures the search was repeated, generating this time 50 000 structures. Also, an additional CSP search for the pair of conformers giving the best agreement in terms of the NMR experiment was performed in the 11 most common space groups (apart from the ones for which a search had already been done), *i.e.* $P2_1/c$, $C2/c$, $P2_12_12_1$, $Pbca$, $Pna2_1$, Cc, $Pnma$, $P1$ and $C2$. The plots presented in the paper show CSP search results from the first stage (with generation of 10 000 crystal structures), while all the other results are given in the supporting information (Figs. S6 and S7).

2.7. DFT-D2 energy re-ranking of crystal structures and calculations of NMR parameters

In each case the CSP search was followed by density functional theory (DFT)-level optimization using the PBE functional and Grimme D2 dispersion correction scheme (Grimme, 2006), as implemented in *CASTEP* (Clark *et al.*, 2005). First, all atomic positions were allowed to relax, while unit-cell parameters were kept rigid, then also unit-cell para-

meters were allowed to relax. For each optimization 600 eV energy cut-off on the plane-wave basis set and k-point spacing of 0.07 Å^{-1} were used. These parameters had been primarily tested for convergence. The number of structures selected for DFT optimization was equal to 14 and 42 for form II and form I, respectively. For the selection criteria see Section 3.

After DFT optimization NMR parameters were calculated using GIPAW methodology (Pickard & Mauri, 2001; Yates *et al.*, 2007) and the same level of theory as described above. The obtained theoretical shielding constants (σ_{calc}) were recalculated to chemical shifts (δ_{calc}) using the following equation: $\delta_{calc} = (\sigma_{calc} - b)/m$, where b and m are the intercept and slope, respectively, obtained after plotting experimental chemical shifts and theoretical shielding constants and calculating the linear regression curve. Subsequently, the root-mean-square (RMS) deviation was calculated for each data set.

2.8. Structural analysis and visualization software

The molecular Hirshfeld surfaces (HS) (Spackman & Jayatilaka, 2009; McKinnon *et al.*, 2007) were calculated from crystal structure coordinates using *CrystalExplorer* software (Turner *et al.*, 2017) and used to highlight the differences in the molecular environments. The surfaces were constructed based on the electron distribution calculated as the sum of spherical atom electron densities. The normalized contact distance (d_{norm}) based on both d_e (the distances from the surface to the closest atom outside the surface) and d_i (the distances from the surface to the closest atom inside the surface), and the van der Waals radii (r) of atoms is given by the equation: $d_{norm} = [(d_i - r_i)/r_i] + [(d_e - r_e)/r_e]$. To visualize molecular packing in the analyzed crystal structures both *CrystalExplorer17* (Turner *et al.*, 2017) and *Chimera* 1.12 (Pettersen *et al.*, 2004) software were used.

The interaction energy calculations were performed using the *CrystalExplorer17* software (Turner *et al.*, 2017) using crystal structures from the obtained cif files as inputs. In each case a cluster with radius of 3.8 Å around a molecule present in the asymmetric unit was generated. The neighboring molecules in the shell around the central molecule were generated by applying crystallographic symmetry operations. The interaction energy calculations (E_{tot}) between symmetry-independent molecules in the crystalline environment were obtained from monomer wavefunctions calculated at the CE-B3LYP/6-31G(d,p) level of theory with the following scaling factors to determine E_{tot}: $k_{ele} = 1.057$, $k_{pol} = 0.740$, $k_{dis} = 0.871$ and $k_{rep} = 0.618$ (Mackenzie *et al.*, 2017). The energies are expressed in terms of electrostatic (E'_{ele}), polarization (E'_{pol}), dispersion (E'_{dis}) and exchange repulsion (E'_{rep}) terms. The total energy (E_{tot}) is represented as $E_{tot} = k_{ele}\,E'_{ele} + k_{pol}\,E'_{pol} + k_{dis}\,E'_{dis} + k_{rep}\,E'_{rep}$, where k values are the scale factors. The magnitudes of the intermolecular interaction energies were graphically represented using energy frameworks, in which the topology of interactions may be conveniently described as a network of tubes connecting centers of molecules. The tube width is proportional to the energy of interaction, while its color depends on the nature of the interaction energy. Tables S3–S5 present energy frameworks corresponding to the different energy components and the total interaction energy in both furazidin forms.

3. Results and discussion

3.1. Preliminary experimental results for forms I and II of furazidin

So far the only known crystal structures of furazidin are its two solvates – monohydrates, one with tetrahydrofuran [Cambridge Crystallographic Data Centre (CCDC) refcode ASATIZ] and one with *N*,*N*-dimethylformamide (CCDC refcode ASATOF) (Bērziņš *et al.*, 2016), but patent literature indicates that there are two neat polymorphs of this API (patent No. WO 2015/181741A1). Our crystallization attempts did not yield any crystallographic quality monocrystals, resulting only in microcrystalline powders. Their identities with forms I and II of furazidin were confirmed with powder X-ray diffraction.

The ^{13}C CP/MAS spectra of both polymorphs, as well as of the DMF solvate-monohydrate (Fig. 2), suggest that form I has

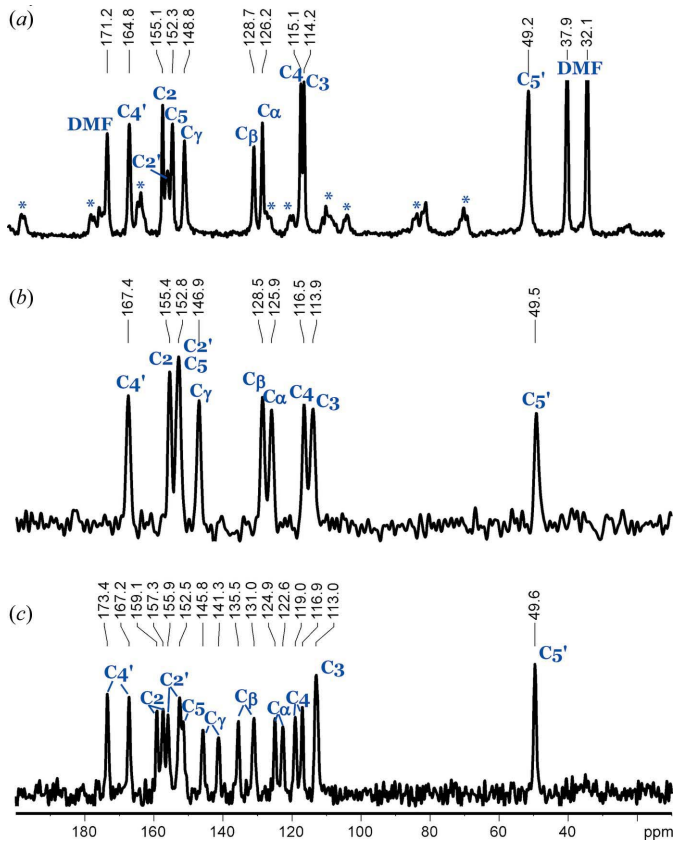

Figure 2
^{13}C CP/MAS NMR spectra with ^{13}C signal assignment of three crystalline forms of furazidin: DMF solvate monohydrate (*a*), form II (*b*) and form I (*c*). Asterisks in the DMF solvate spectrum mark spinning sidebands. Note that this spectrum was registered with 10 kHz spinning speed, whereas spectra shown in (*b*) and (*c*) were registered with 60 kHz spinning speed, and so spinning sidebands for these spectra are outside the observed spectral region.

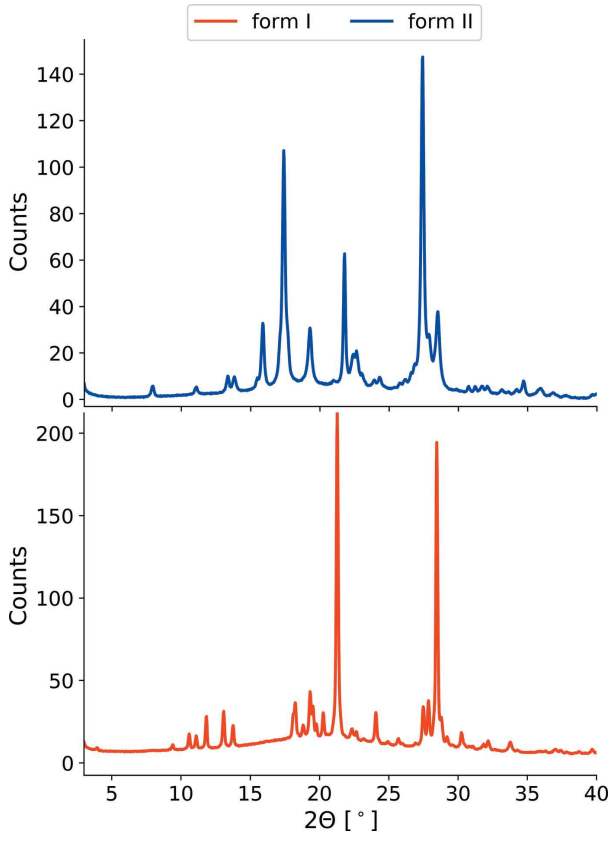

Figure 3
Powder X-ray diffractograms for forms I and II of furazidin.

two molecules in the asymmetric part of a unit cell, visible as a doubling of almost all observed ^{13}C resonances. Form II, on the other hand, seems to be very similar to the DMF solvate-monohydrate in terms of ^{13}C NMR chemical shifts, with only one symmetry-independent molecule. In contrast, both neat forms display very similar thermal behavior, with decomposition observed at temperatures 289 and 288°C for forms I and II, respectively (for DSC plots see Fig. S2).

3.2. Conformational search

Furazidin is a fairly rigid molecule with only three rotatable bonds marked with gray arrows in Fig. 1. Its conformational search yielded 22 conformers, which after re-optimization at the DFT level of theory gave a final eight distinct conformers with the highest relative gas-phase energy with respect to the best one being equal to 22.5 kJ mol^{-1}. This means that all eight conformers can form stable crystal structures (Thompson & Day, 2014).

3.3. Extracting experimental constraints

Powder X-ray diffractograms of forms I and II are given in Fig. 3. Indexing of the PXRD diffractogram of form II yielded three plausible unit cells, one belonging to monoclinic, and the other two to triclinic crystal systems. The first unit cell with parameters being equal to a = 11.62, b = 11.42, c = 8.48 Å and β = 106.91° should contain four molecules of furazidin to yield a probable density of 1.63 g cm^{-3}, which means four symmetry operations. Hence the most probable space groups are *Cm*, *Cc*, *P*2/*c*, *C*2/*m*, *P*2/*m*, *P*2$_1$/*m*, *P*2$_1$/*c*, *C*2/*c*. Of these *P*2$_1$/*c* and *C*2/*c* are the most common ones, and their Pawley refinement against the experimental diffractogram yielded R_{wp} equal to 8.47%. The unit cells belonging to a triclinic crystal system gave somewhat worse agreement with the PXRD experiment, with R_{wp} values obtained after Pawley refinement equal to 9.63% and 10.0% for cells with parameters a = 11.49, b = 8.59, c = 8.52 Å, α = 66.95°, β = 104.79°, γ = 96.62° (d = 1.17 g cm^{-3}) and a = 11.13, b = 8.46, c = 8.13 Å, α = 104.37°, β = 90.43°, γ = 92.96° (d = 1.18 g cm^{-3}), respectively. As a result it seems most reasonable to do a CSP search first in *P*2$_1$/*c* and *C*2/*c* space groups, followed by a search in *P*1 and *P*$\bar{1}$ space groups.

In the case of form I PXRD diffractogram indexing gave two possible unit cells, in monoclinic and triclinic crystal systems. The obtained cell parameters for the mentioned crystal systems were equal to a = 22.63, b = 6.54, c = 9.72 Å, β = 99.47°, which corresponds to a density of 1.24 g cm^{-3} for four furazidin molecules, and a = 10.79, b = 9.98, c = 8.33 Å, α = 64.98°, β = 110.13°, γ = 117.27°, corresponding to a density of 1.24 g cm^{-3}. The R_{wp} values for both unit cells obtained after Pawley refinement were equal to 5.54 and 10.8%, respectively. Hence the most probable space groups for this polymorphic form are *P*2, *P*2$_1$, *Pm*, *Pc*, *P*1 and *P*$\bar{1}$.

The next experimental constraint, which can significantly facilitate CSP search, is the conformation of a compound in a crystal. One of the best ways to extract constraints enabling determination of a conformer is via solid-state NMR measurements under very fast magic-angle spinning (VF MAS), *i.e.* with a spinning speed of at least 42 kHz. In such conditions it is usually possible to reliably assign all ^{1}H

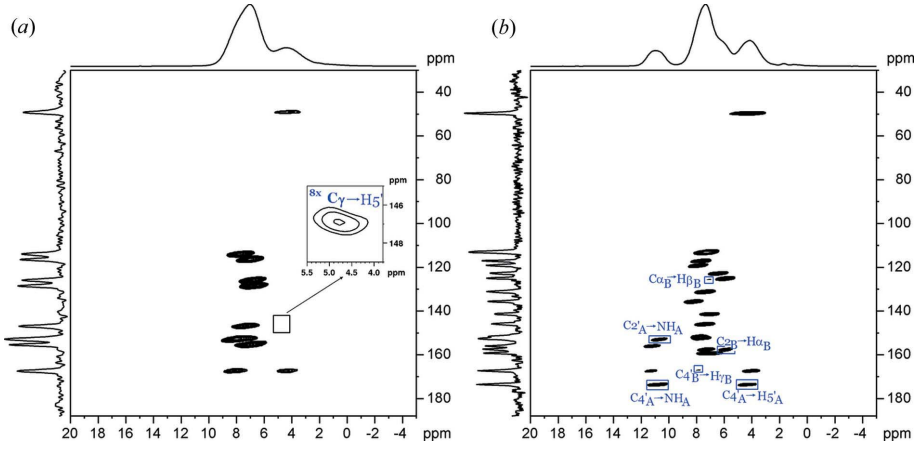

Figure 4
^{1}H–^{13}C invHETCOR spectra with long contact time registered at the spinning speed of 60 kHz for forms II (*a*) and I (*b*) with assigned crucial correlation peaks.

and ^{13}C resonances, as well as to determine additional ^{1}H–^{13}C or ^{1}H–^{1}H through-space correlations, which arise from proximities of certain atoms in a molecule or in a crystallographic unit cell. Fig. 4 shows ^{1}H–^{13}C invHETCOR correlation spectra with long contact time, registered at 60 kHz spinning speed for both polymorphs, while their ^{1}H and ^{13}C chemical shifts can be found in Table S1. ^{1}H and ^{13}C signal assignment for form II is quite a straightforward task and does not create any difficulties. In addition a correlation between Cγ and H5′a indicates that these atoms must be close in space, a condition which is fulfilled only by four out of eight conformers.

In the case of form I, the analysis of its 2D spectra proves that there are indeed two symmetry-independent molecules, as suggested before by 1D NMR measurements. The observed ^{1}H–^{13}C correlations allow us to assign all resonances to respective atoms in furazidin molecules, but there are some ambiguities as to the full assignment to each molecule separately. For example, it is possible to allocate resonances originating from C2′, C4′, C5′, Cγ, Hγ, H5′ and NH to molecules *A* and *B*, as well as to identify correlations between Cα, Cβ, C2, C3, C4, C5 and their corresponding protons, but the correlations which could help to combine those two groups together and thus enable the full assignment to molecules *A* and *B* are inconclusive due to signal overlap. As a result we decided to check parameters calculated for theoretical structural models against two possible combinations of the assignment. As for additional structural constraints there is a weak correlation, which can be assigned to C5′ and Hγ, suggesting that, again, the same four conformers should be accounted for primarily. However, in this case it is also possible that this correlation originates from a different proton than Hγ, as its resonating frequency is close to those found for other ^{1}H atoms. It is also unclear whether this structural constraint should be used for one or for both molecules. As a result it seems more reasonable not to exclude any conformer and do a CSP search for all possible combinations of conformers (*i.e.* 36 combinations), but limit the searched space groups from among those indicated by PXRD indexing to the most common ones, that is $P\bar{1}$, $P2_1$ and *Pc*.

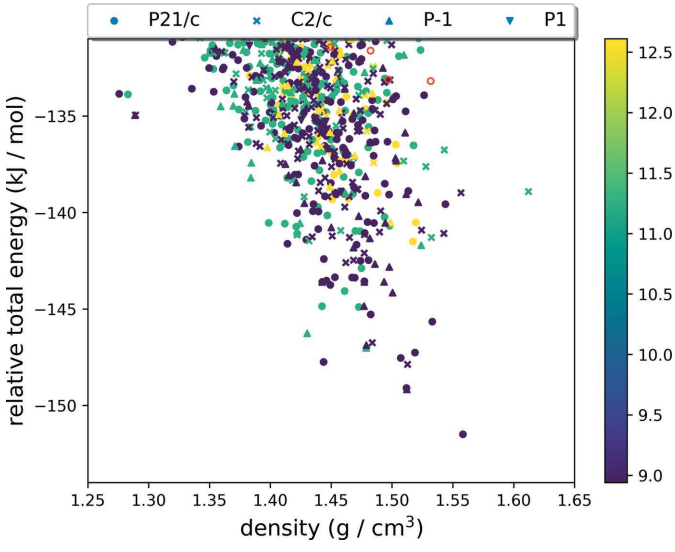

Figure 5
CSP energy landscape for four possible conformers tested in $P2_1/c$, $C2/c$, $P1$ and $P\bar{1}$ space groups for the $Z' = 1$ polymorph of furazidin (form II). Structures obtained for different conformers are color-coded according to their gas-phase energy in kJ mol^{-1}, as shown in a color bar, except for the highest-energy gas-phase conformer, which is shown in red.

Apart from the structural constraints, which can be used in the selection of plausible conformers, solid-state NMR spectra can deliver information on the intermolecular close contacts. In the majority of cases it is impossible to distinguish *a priori* which correlations arise from intramolecular interactions (information on the conformation of a molecule), and which from intermolecular ones (information on mutual arrangement of molecules inside a crystal). However, this is not the case if there are two molecules in the asymmetric part of a crystallographic unit cell and visible correlation signals arise from the same nuclei in distinct molecules. Obviously, such correlations can only be the result of intermolecular interactions, thus giving additional structural constraints, which cannot be used before a CSP search, but can allow for the elimination of the CSP-generated model structures which do not fulfill these constraints. This is the case for furazidin form I. In its ^{1}H–^{1}H Back-to-Back correlation spectrum there is a clearly visible correlation between two protons resonating at 10.8 and 11.3 p.p.m. (see Fig. S5). These signals originate from amide (NH) protons in molecules A and B, respectively. As a result, these two protons have to be close in space in the crystal of form I.

Summarizing this part, we were able to successfully narrow down the number of possible space groups which should be accounted for in a CSP search for forms I and II of furazidin, as well as to narrow down to four the number of possible conformers that can be present in the crystal structure of form II. In addition we were able to extract an additional structural constraint for form I, which can be used after the CSP search, *i.e.* close proximity of NH_A and NH_B protons.

3.4. CSP search for form II ($Z' = 1$)

The CSP crystal energy landscape for four selected conformers in $P2_1/c$, $C2/c$, $P1$ and $P\bar{1}$ space groups is shown in Fig. 5. The lowest-energy region of this plot, which is the first 20 kJ mol^{-1} above the global minimum, is very crowded with more than 500 distinct crystal structures. Eight lowest-energy structures, including the landscape's global minimum, are built using a conformer with the lowest gas-phase energy among the tested ones, with intermolecular energy 8.94 kJ mol^{-1} above the global gas-phase minimum. All the other conformers build significantly less favorable structures, with the best one being 5 kJ mol^{-1} higher in energy than the global minimum structure. It is noteworthy that all structures built by the highest-energy conformer (with gas-phase energy 22.5 kJ mol^{-1} higher than the gas-phase global minimum, marked in red in Fig. 5) are very high in total energy, with the best one having its total energy 18 kJ mol^{-1} higher than the CSP landscape

global minimum. This suggests that all conformers of furazidin are able to pack quite efficiently in a crystal structure, and the factor that determines their final energy is primarily intramolecular energy contribution (*i.e.* gas-phase energy of a conformer).

As for the space group, the most energetically favorable structures seem to be those in the $P2_1/c$ space group, but those found in $C2/c$ and $P\bar{1}$ are only slightly less favorable. The global minimum structure, with total energy only 1.5 kJ mol^{-1} lower than the energy of the second best structure, has unit-cell parameters equal to $a = 11.66$, $b = 11.94$, $c = 8.47$ Å and $\beta = 107.22°$, in close agreement with one of the possible unit cells indicated by indexing the powder X-ray diffractogram. However, to further evaluate whether this structure is the one observed experimentally, it needs to be re-optimized, having NMR parameters calculated and compared with experimental ones. In addition, we also decided to calculate NMR parameters for the lowest-energy structures of each conformer in each of the tested space groups to check the level of agreement for as wide variety of structures as possible and determine whether there will be a significant difference in the agreement between this structure and all the others.

The re-optimization of the selected model structures at the DFT-D2 level of theory resulted in changes in the final energy ranking. After re-optimization the force field global minimum structure was now found to be the third best structure, with relative total energy 1.7 kJ mol^{-1} higher than the DFT-D2 global minimum. This energy difference, however, is well within error boundaries of the applied dispersion correction scheme. As for the ^{1}H and ^{13}C RMS values, which express the level of agreement between experimental and theoretical NMR parameters, the force field global minimum structure is unquestionably the one showing the best agreement with the NMR experiment, with 0.3 and 2.6 p.p.m. for ^{1}H and ^{13}C RMS, respectively (see Fig. 6). This confirms our previous assumption that this structure is the one observed experimentally. Final proof is delivered by Rietveld refinement of this structure against the experimental powder X-ray diffractogram, which yielded a very good R_{wp} value of 9.60% (for the comparison of simulated and experimental PXRD diffractograms see Figs. S7 and S8). Note that, from now on, throughout the paper we refer to this structure as the experimental one for form II. By doing so we mean that this is the structure actually observed in the laboratory for form II of furazidin, but it was obtained via theoretical methods and then confirmed and refined by the performed solid-state NMR and PXRD experiments.

It is worth noting that the structure indicated as the one of form II is actually the only one having low RMS values for both tested nuclei, while some of the other model crystal structures have quite a low RMS value for ^{1}H only or ^{13}C only. For example, the 16th structure (according to its DFT-D2 energy rank), with relative total energy as high as 33.8 kJ mol^{-1} above the DFT-D2 global minimum, has a surprisingly low ^{1}H RMS value, equal to 0.39 p.p.m. This structure, however, apart from being too far from the energetic global minimum to be designated as the experimental one, shows very poor agreement with the experiment in terms of ^{13}C NMR values, with an RMS equal to 5.8 p.p.m. In our previous studies we have shown that the sensitivity of ^{1}H NMR parameters to local changes in the chemical environment of a crystal is usually significantly higher than the sensitivity of ^{13}C NMR data, and is indicative of a molecular conformation inside the crystal, rather than crystal packing itself (Dudek *et al.*, 2016, 2017). In the case of furazidin, however, looking only at ^{1}H NMR data seems to be not enough to unambiguously indicate the correct structural model, and this may be due to at least two factors. First is the presence of two carbonyl groups, the chemical shifts of which are very sensitive to intermolecular interactions, and second is the fact that furazidin has limited conformational freedom, with the obtained conformers being similar to each other in terms of chemical environment around particular nuclei. As a result it is more probable that serendipitous agreement with the experiment will be observed for one of the regarded nuclei, but it is unlikely that this will be the case for both nuclei (^{1}H and ^{13}C).

Bearing this in mind, we decided to examine all cases of false-positive indications in terms of ^{1}H RMS values, that is all model crystal structures with a low ^{1}H RMS value, but not

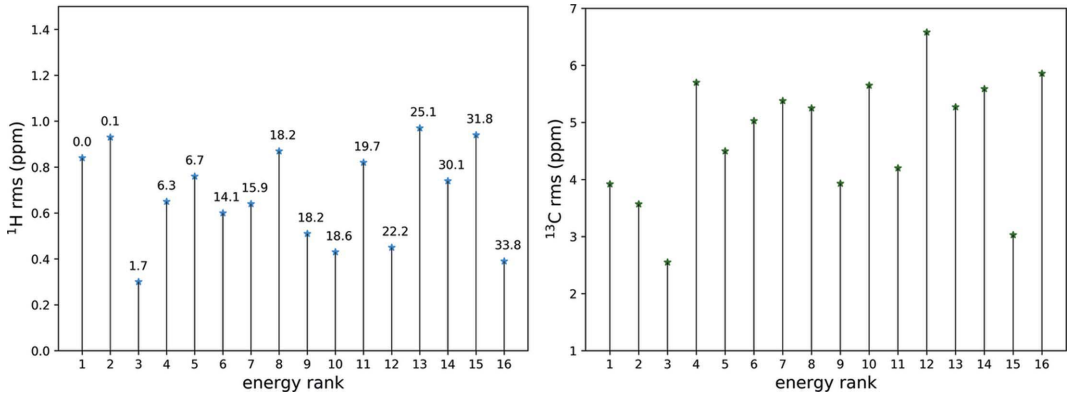

Figure 6
^{1}H and ^{13}C RMS values (in p.p.m.) obtained after comparison of experimental and theoretical NMR parameters for the selected model crystal structures obtained from CSP search for four conformers in $P2_1/c$, $C2/c$, $P\bar{1}$ and $P1$ space groups. The annotated values in the ^{1}H RMS plot represent relative total DFT-D2 energies of the model crystal structures (in kJ mol^{-1}, calculated per one furazidin molecule) with respect to the lowest-energy structure.

being the one observed experimentally. Apart from the experimental crystal structure, there are four model crystal structures with a ^{1}H RMS value equal to or lower than 0.5 p.p.m., a level of agreement which in the absence of all other data might be considered enough to prove an identity with the experimental crystal structure (Hofstetter & Emsley, 2017; Baias, Widdifield *et al.*, 2013). These are 9th, 10th, 12th and 16th structures with ^{1}H RMS values equal to 0.51, 0.43, 0.45 and 0.39 p.p.m., respectively. Only the 9th structure, found in the *P*1 space group, is built by the same conformer as the experimental structure and it has seven out of 15 molecules in common with the experimental structure with an RMS value of 0.148 Å when compared with the *Crystal Packing Similarity Tool* (Chisholm & Motherwell, 2005), using default comparison parameters (15-molecule cluster, geometrical tolerance of 20% for atomic distances and 20° for angles). In both structures furazidin molecules form layers held together by N—H···O intermolecular hydrogen bonds, and in both cases furazidin molecules are arranged in the same way within each layer, but there is a different arrangement of the layers with respect to each other. The other three structures with low ^{1}H RMS are built by different conformers than the experimental structure, showing that in the case of furazidin the agreement in terms of ^{1}H NMR data is not necessarily indicative of a conformation inside the crystal. In contrast, in all of them furazidin molecules interact via N—H···O intermolecular hydrogen bonds, a feature not observed in crystal structures with much worse agreement in terms of ^{1}H NMR data. On the other hand, the same hydrogen-bonding interactions seem to exhaust the list of similarities between the compared crystal structures. As an example, Fig. 7 shows the arrangement of furazidin molecules in the experimental crystal structure and the 16th crystal structure, which is the one with the next best agreement in terms of ^{1}H NMR data. In this case both furazidin molecules within one layer, as well as mutual arrangement of layers interacting via short contacts are different for both structures, which is reflected by a disagreement in terms of ^{13}C NMR data for the 16th structure.

In summary, it can be concluded that the agreement in terms of ^{1}H solid-state NMR data alone may in some cases be serendipitous (though it usually is associated with some similarities with the experimental structure), and as such is not enough to prove the identity of the examined crystal structure. However, if this indeed is the case, it should be reflected by a disagreement in terms of ^{13}C NMR data. Lastly, as it is difficult to decide *a priori* what agreement in terms of the NMR data is good enough, it is necessary to account also for relative total energy of a regarded structure. Its value indicates the most favorable (and therefore the most probable) arrangement of molecules inside a crystal structure. Therefore, a model crystal structure with good agreement in terms of NMR parameters cannot be regarded as the experimental one if its relative total energy is significantly higher than that for some of the other structures.

3.5. CSP search for form I (Z' = 2)

The computational search for the crystal structure of form I is a much more demanding task than the one for form II. As pointed out in Section 3.3 it was not possible to exclude any conformation on the basis of experimental constraints (with only a slight indication to a conformation similar to the one found in the crystal structure of form II), which means that 36 possible combinations of all eight conformers had to be tested at least in three selected space groups, *i.e.* in $P2_1$, *Pc* and $P\overline{1}$. The lowest-energy region of the resulting CSP crystal energy landscape is shown in Fig. 8. In this case, as was similarly observed for the Z' = 1 polymorph, the majority of low-energy structures are built by low-energy gas-phase conformers, although here the effect is not as strong as it was for form II. Clearly, the formation of a Z' = 2 crystal structure can result in stronger intermolecular interactions, thus enabling Z' = 2

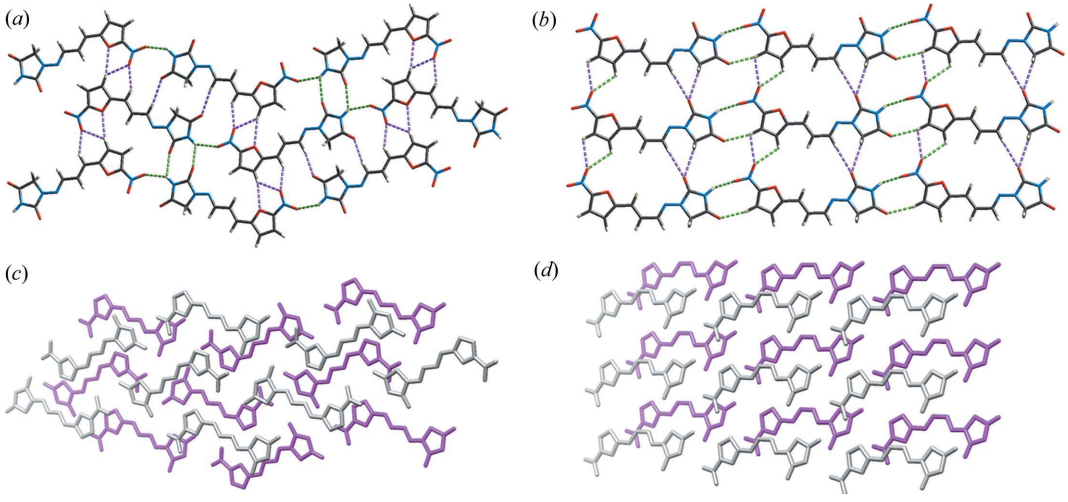

Figure 7
Molecular arrangement of furazidin molecules in the Z' = 1 polymorph (form II): the experimental crystal structure (*a*) and (*c*) and 16th (according to its DFT-D2 energy rank) theoretical crystal structure (*b*) and (*d*). The upper panel (*a*) and (*b*) shows the arrangement within one layer, N—H···O hydrogen bonds are marked with green dotted lines, short C—H···O contacts with purple dotted lines; the lower panel (*c*) and (*d*) shows the inter-layer arrangement, with two interacting layers represented by different colors.

structures to be built by less energetically favored conformers. As to the space-group preferences, it seems that there is almost an equal distribution of structures in all three tested space groups in the lowest-energy region of the landscape.

The observed global minimum on the force field landscape belongs to the structure found in the $P2_1$ space group, with unit-cell parameters equal to a = 9.62, b = 11.26, c = 11.21 Å and β = 102.79°, different from those indicated by indexing of the experimental PXRD diffractogram for form I of furazidin. Therefore, this time global minimum structure is probably not the one observed experimentally. In a search for the experimental crystal structure a comparison with the NMR experiment of the most plausible candidates would be of use. However, the low-energy region of the CSP landscape for the

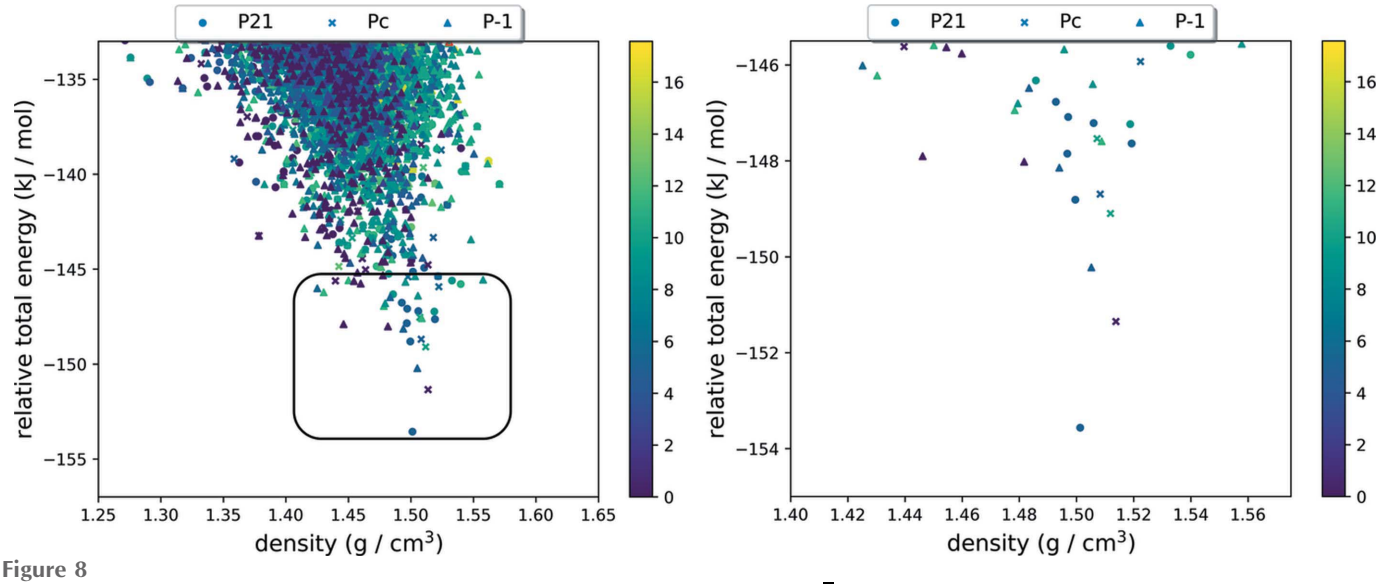

Figure 8
CSP energy landscape for all possible combinations of conformers tested in $P2_1$, Pc and $P\bar{1}$ space groups for the Z' = 2 polymorph of furazidin (form I). Structures obtained for different conformers are color-coded according to their gas-phase energy in kJ mol^{-1} (which is an averaged value for two conformers present in each structure), as shown in a color bar. The black rectangle indicates the expansion region shown at the right-hand side of the figure.

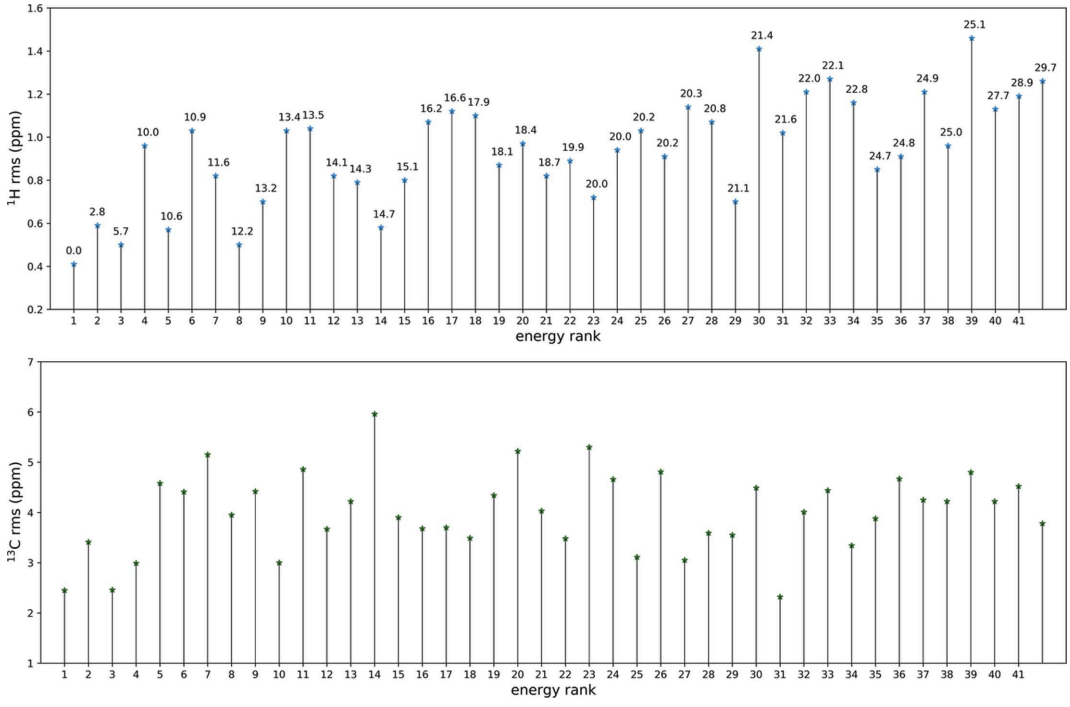

Figure 9
^{1}H and ^{13}C RMS values (in p.p.m.) obtained after comparison of experimental and theoretical NMR parameters for the selected model crystal structures obtained from CSP search for the furazidin Z' = 2 polymorph (form I) – the search has been performed for 36 conformers in $P2_1$, Pc and $P\bar{1}$ space groups. The annotated values in the ^{1}H RMS plot represent relative total DFT-D2 energies of the model crystal structures (in kJ mol^{-1}, calculated per one furazidin molecule) with respect to the lowest-energy structure.

$Z' = 2$ polymorph is even more crowded than was observed for form II, with over 3600 structures having relative total energy of less than 20 kJ mol^{-1} above the global minimum. Obviously, re-optimization of such a number of structures with the DFT-D2 method would consume a prohibitively large amount of computational time. Instead, we decided to re-calculate at this level of theory only the lowest-energy structures for each conformer in each of the tested space groups which had total relative energy lower than 15 kJ mol^{-1} above the global minimum. This procedure, followed by NMR parameter calculations, should indicate which of the tested structures are close in terms of NMR data to the experimentally observed structure. Then, if needed, a more exhaustive search for the most promising candidates can be performed.

The above-presented criteria resulted in the selection of 42 possible crystal structures, built by 18 different combinations of conformers. As expected, their re-optimization somewhat changed the energy ranking, so that now the DFT-D2 global minimum structure is the one found in the $P\overline{1}$ space group, with unit-cell parameters of $a = 22.44$, $b = 12.45$, $c = 5.33$ Å, $\alpha = 50.96$, $\beta = 92.50$, $\gamma = 97.02°$. These parameters bear some resemblance to the ones obtained for a monoclinic crystal system from indexing of the PXRD diffractogram for form I (see Section 3.3). Rietveld refinement performed for this structure yielded a very good agreement of $R_{wp} = 13.23\%$ (for the comparison of experimental versus simulated PXRD diffractograms see Fig. S9). As a result this structure can be considered the experimental one (the one observed in the laboratory for form I of furazidin), provided that it shows a very good agreement with the NMR experiment.

Fig. 9 presents the ^{1}H and ^{13}C RMS values obtained after comparison of theoretical and experimental NMR data for 42 model crystal structures. Indeed, the global minimum structure shows the best agreement in terms of ^{1}H chemical shifts, with an RMS value equal to 0.41 p.p.m. and the second best in terms of ^{13}C chemical shifts (RMS = 2.45 p.p.m.). Note that, in terms of the ^{1}H RMS value, this agreement seems to be worse than the one obtained for form II of furazidin, but this is not the case when looking at the correlation coefficient (R^2) obtained from linear regression. In fact, the R^2 value for furazidin form I is equal to 0.963, while for form II it is equal to 0.955 (for R^2, RMS, slope and intercept values of all the calculated structures see Table S8). This structure is built by a pair of identical conformers, forming dimers interacting via C—H···O hydrogen bonds (Fig. 10). As a result the NH protons of both symmetry-independent molecules are in close proximity, with a distance of only 2.52 Å. Therefore, this structure also fulfills the intermolecular structural constraint extracted from the ^{1}H–^{1}H BaBa (Back-to-Back) NMR spectrum. It is noteworthy that the conformer found in this structure belongs to the same group of conformers as the one found in form II of furazidin, which was also suggested by the results of solid-state NMR measurements. Given all the above evidence, we conclude that the DFT-D2 global minimum structure is the experimental structure of form I. From now on we will refer to this structure as the experimental one, as was justified previously for the structure obtained for form II.

As a side note, it is worth pointing out that indexing of the PXRD diffractogram of form I did not yield the unit cell, which was eventually found for the experimental structure, but only a similar one, found in a different crystal system. This is not surprising if we consider that molecules which do not readily form crystallographic quality monocrystals often have a tendency to show a rather poor degree of crystallinity, a feature that can significantly influence the quality of PXRD data.

As before, it is worthwhile looking at all the other model crystal structures giving good agreement in terms of NMR parameters. Among 42 tested structures there are six structures having a ^{1}H RMS value lower than 0.6 p.p.m.: the experimental crystal structure, second, third, fifth, eighth and 14th crystal structures (the numbering of structures is given according to their DFT-D2 energy ranks). Of these only two crystal structures also have good agreement in terms of ^{13}C NMR data, with the RMS value lower than 3.0 p.p.m.: the experimental structure and the third crystal structure. This latter structure, found in the $P2_1$ space group, is built by exactly the same pair of conformers as the experimental one, displays a similar, though not identical, hydrogen-bonding pattern [Fig. 10(*b*)] and has six out of 15 molecules in common with the experimental structure (RMS = 0.456 Å), when compared using the *Crystal Packing Similarity Tool* (Chisholm & Motherwell, 2005) and default comparison parameters. It also fulfills the condition of close proximity of NH_A and NH_B protons (with the N—H···N intermolecular distance equal to 2.99 Å). These similarities explain the agreement in terms of NMR parameters observed for this structure. Out of the remaining four model crystal structures having good agree-

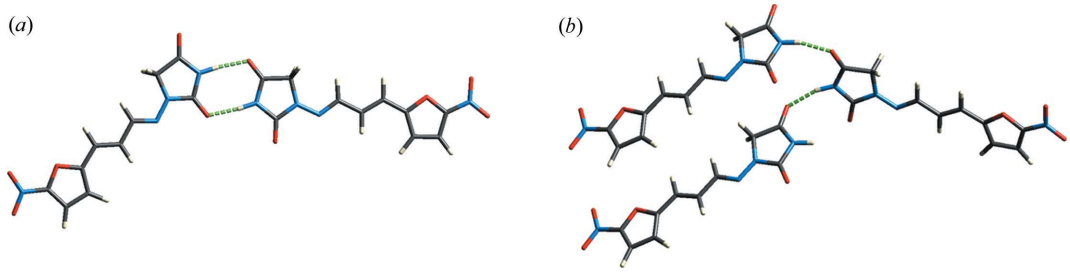

Figure 10
Hydrogen-bonding pattern in the experimental crystal structure of form I (*a*) and in the third-lowest-energy crystal structure (*b*), built by the same conformers as the experimental structure; hydrogen bonds are marked with dotted green lines.

Table 1
Comparison of unit-cell parameters for crystal structures of furazidin forms I and II obtained after force field and DFT-D2 geometry optimization, as well as after Rietveld refinement.

The obtained cif files are available as supporting information either in their native cif format (for Rietveld refined structures) or as plain text files (for other cif files).

Unit-cell parameters	Force field optimized structure	DFT-D2 optimized structure	Rietveld refined structure
Form I			
a b c (Å)	22.388 12.654 5.334	22.440 12.655 5.334	22.183 (22) 12.546 (7) 5.3092 (16)
$\alpha\ \beta\ \gamma$ (°)	50.937 92.532 97.159	50.957 92.507 97.022	51.074 (3) 92.16 (3) 97.31 (11)
Form II			
a b c (Å)	11.659 11.944 8.466	11.898 11.636 8.467	11.670 (7) 11.4666 (12) 8.494 (4)
β (°)	107.22	106.65	106.848 (14)

ment in terms of ^{1}H NMR data, three contain at least one conformer identical to the experimental crystal structure, and the 8th crystal structure displays the same hydrogen-bonding pattern, fulfills the NH_A and NH_B proximity condition, and has six out of 15 molecules in common with the experimental structure (RMS = 0.626 Å). Only the 14th crystal structure is different from the experimental structure in terms of both conformers building this structure and its hydrogen-bonding pattern. This manifests itself in a poor agreement in terms of ^{13}C NMR data, which actually is the worst from among the tested structures and equal to 5.96 p.p.m.

To conclude this part, in the case of form I the agreement in terms of ^{1}H NMR data is more indicative of similarities of the regarded model crystal structures with the experimental one than was the case for form II. These similarities concern primarily the conformation of a molecule found inside the crystal and/or similar hydrogen-bonding interactions. However, serendipitous agreement in terms of ^{1}H only or ^{13}C only RMS data, but not in terms of both, was also observed for this form.

3.6. Comparison of Z' = 1 (form II) and Z' = 2 (form I) polymorphs

DSC measurements for both neat polymorphs of furazidin indicate that they have similar thermal stability, which at the same time is a measure of their enthalpy of formation. Therefore, we can expect that their total energies obtained from quantum chemical calculations will also be similar. This indeed is the case. In the force field crystal energy landscape crystal structures identified as forms I and II are separated by 4 kJ mol^{-1}, with form II having lower total energy than form I, but after the DFT optimization this trend was reversed, and form I was found to be more energetically stable than form II, with total DFT energy 1.6 kJ mol^{-1} lower. Regardless of the level of theory used, the observed differences in energy are small and support the existence of these two polymorphic forms. Table 1 summarizes changes to the unit-cell parameters in the crystal structures of furazidin forms I and II obtained from force field (CSP) calculations, after DFT-D2 geometry optimization, as well as after Rietveld refinement of the computationally generated structures against respective powder X-ray diffraction patterns. As can be seen, optimization of the CSP-generated structures at a higher level of theory (DFT-D2) did not change the unit-cell parameters significantly, with Rietveld refinement having a more noticeable impact on the regarded parameters. All cif files corresponding to the described crystal structures are available as supporting information files.

The lowest-energy region of the force field crystal energy landscape for Z' = 1 and Z' = 2 crystal forms [first 10 kJ mol^{-1} above the global minimum, Fig. 11(*d*)] contains a significantly larger amount of Z' = 2 structures. This is probably the result of a larger number of possible packing arrangements, but it may also originate from a better energetic compensation offered by the possibility of formation of Z' = 2 structures, as pointed out before. A comparison of form I and form II structures [Figs. 11(*a*) and 11(*b*)] indicates that form II is visibly more densely packed (its density after DFT-D2 optimization is equal to 1.563 g cm^{-3}), in comparison with form I (d = 1.506 g cm^{-3}), and yet this latter form has lower DFT-D2 energy. On the other hand, the conformer found in this form has relative gas-phase energy 11.94 kJ mol^{-1} higher than the global minimum, which is only 3 kJ mol^{-1} higher than is the case for form II [for an overlay of furazidin molecules see Fig. 11(*c*)]. This means that the intermolecular energy contribution to the total energy of form I is 4.6 kJ mol^{-1} higher than that of form II. This in part supports the conclusion that the Z' = 2 structure offers furazidin molecules more favorable intermolecular interactions and therefore a better energetic compensation. The differences in molecular environment of a single furazidin molecule in both polymorphs are highlighted by Hirshfeld surfaces shown in Fig. S11, while the calculated energy frameworks showing the contribution of dispersion and electrostatic energies to the total energies of the crystals are shown in Table S7. Although both polymorphs of furazidin are structurally distinct, their global interaction topologies are apparently comparable as evident from energy framework analysis (see Tables S3–S7).

Finally, we would like to point to similarities of supramolecular synthons present in two polymorphs of furazidin with the synthons observed in two crystal structures of a similar molecule. As mentioned before, in the CCDC database no crystal structures of neat furazidin have been published so far. There are however crystal structures of nitrofurantoin, which differs from furazidin only in the length of a carbon chain

linking tetrahydrofuran and hydantoin rings. Nitrofurantoin, similarly to furazidin, has two polymorphic forms, a triclinic one and a monoclinic one. These polymorphs, designated as α and β forms, crystallize in $P\overline{1}$ and $P2_1/n$ space groups, respectively (the respective CCDC refcodes for these structures are LABJON01 and LABJON) (Bertolasi *et al.*, 1993; Pienaar *et al.*, 1993), both with one nitrofurantoin molecule in the asymmetric part of a unit cell. The first of these polymorphs, the triclinic one, displays very similar intermolecular interactions to the triclinic form of furazidin (form I), with dimers interacting via N—H···O hydrogen bonds formed between hydantoin rings (Fig. S11*a*). In contrast, in the β polymorph there are only some supramolecular synthons which are the same as in form II of furazidin, namely N—H···O (carbonyl group) interactions, with no N—H···O (NO_2 group) hydrogen bonds. The main difference in the intermolecular interactions between the two structures lies in the orientation of the regarded molecules: in the monoclinic polymorph of nitrofurantoin the molecules are arranged in a head-to-head manner, where the 'head' is a hydantoin ring (Fig. S11*b*), while in the furazidin monoclinic polymorph there is a head-to-tail arrangement, *i.e.* the NO_2 group substituted to the furan ring is directed towards the hydantoin ring from the second molecule.

4. Conclusions

In this work two previously uncharacterized polymorphs of furazidin were described using NMR crystallography and crystal structure prediction calculations. The described $Z' = 1$ and $Z' = 2$ polymorphic forms display similar thermal and energetic stability and were found to crystallize in $P2_1/c$ and $P\overline{1}$ space groups, respectively. Their structural determination was possible only after combining data from very fast magic-angle spinning solid-state NMR experiments, powder X-ray diffraction and crystal structure prediction calculations. In terms of NMR crystallography application to the structural determination of microcrystalline substances, our results underline the need for caution when analyzing the agreement between theoretical and experimental NMR data, indicating the cases of false-positive matches, especially when accounting for NMR data obtained for only one nuclei (*i.e.* only ^{1}H or ^{13}C). On the other hand, a case in which the NMR data for both nuclei are serendipitously in very good agreement with the experiment has not been observed. It is therefore always advisable to look at both ^{1}H and ^{13}C data when elucidating crystal structure using NMR crystallography. We feel that there is still not enough data in the literature identifying and analyzing cases of false-positive matches in terms of solid-state NMR data and/or dealing with the question of what agreement in terms of NMR data is good enough for different crystal systems ($Z' > 1$ polymorphs, hydrates, solvates, flexible

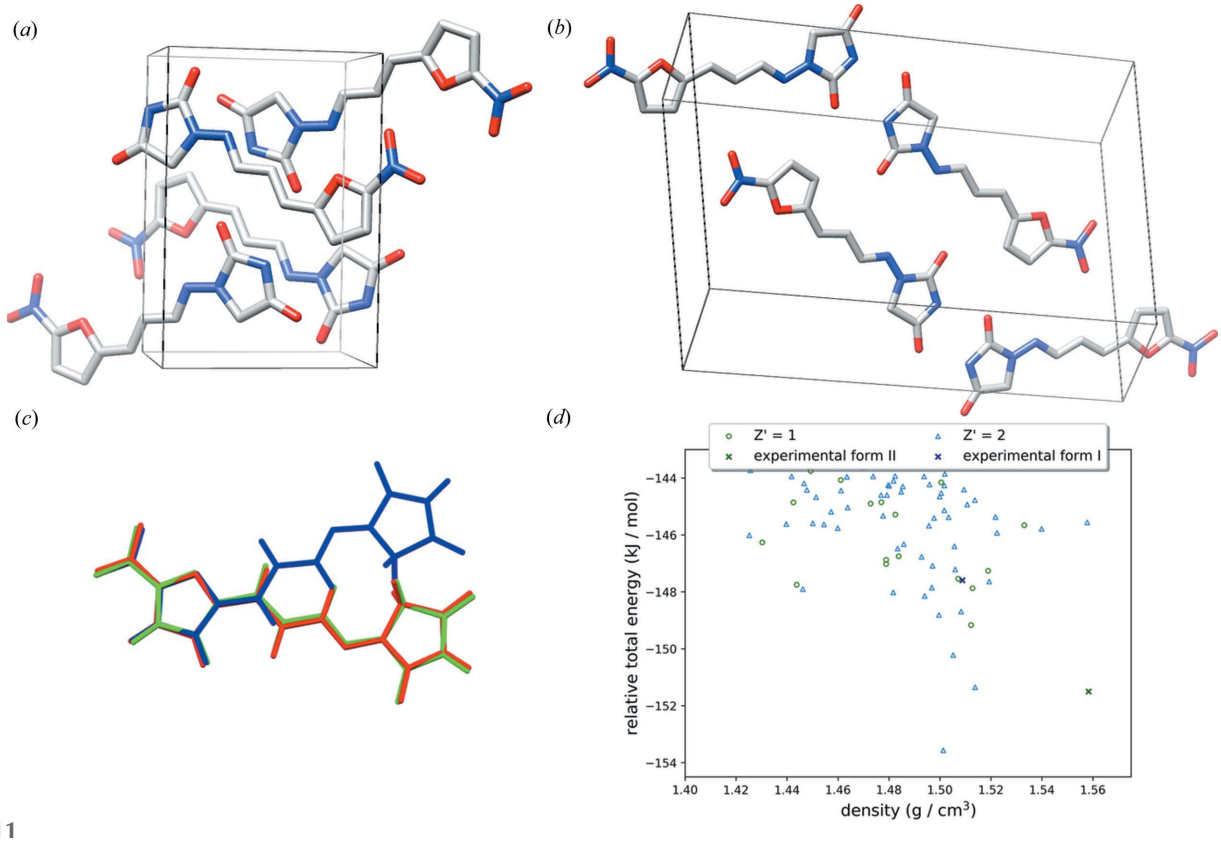

Figure 11
Packing arrangement for the experimental crystal structures of form II (*a*) and form I (*b*) of furazidin, an overlay of furazidin molecules present in form I (red and green) and in form II (blue) (*c*), and the comparison of the lowest-energy region of crystal energy landscapes of $Z' = 1$ and $Z' = 2$ structures of furazidin (*d*).

molecules). Such studies can be a valuable source of information as to what can be expected when using NMR crystallography in crystal structure determination.

In summary, we would like to stress that crystal structure determination from a microcrystalline powder using a CSP–NMR approach is much more difficult when dealing with $Z' > 1$ polymorphs. This concerns almost all stages of the structure determination process, starting from the necessity of accounting for more degrees of freedom in the CSP search (both conformational and in terms of molecule rotations and translations in a crystal), through difficulties in extracting viable structural constraints from NMR experiments (mainly due to the signal overlap), to reliable identification of a correct structure from among the numerous ones generated in the CSP process (mostly due to a larger amount of structures giving reasonably good agreement with the NMR experiment).

Acknowledgements

The authors are very grateful to Wojciech Dudek for his help in the adaptation of the *CSPy* code to the Polish supercomputing infrastructure.

Funding information

This work was financially supported by the Polish National Science Center under Sonata 14 grant No. UMO-2018/31/D/ST4/01995. The Polish Infrastructure for Supporting Computational Science in the European Research Space (PL-GRID) is gratefully acknowledged for providing computational resources. This project has received funding from the European Union's Horizon 2020 research and innovation program under grant agreement No. E190200237 (EUSMI).

References

Althaus, S. M., Mao, K., Stringer, J. A., Kobayashi, T. & Pruski, M. (2014). *Solid State Nucl. Magn. Reson.* **57–58**, 17–21.
Baias, M., Dumez, J.-N., Svensson, P. H., Schantz, S., Day, G. M. & Emsley, L. (2013). *J. Am. Chem. Soc.* **135**, 17501–17507.
Baias, M., Widdifield, C. M., Dumez, J.-N., Thompson, H. P. G., Cooper, T. G., Salager, E., Bassil, S., Stein, R. S., Lesage, A., Day, G. M. & Emsley, L. (2013). *Phys. Chem. Chem. Phys.* **15**, 8069–8080.
Becke, A. D. (1993). *J. Chem. Phys.* **98**, 5648–5652.
Bertolasi, V., Gilli, P., Ferretti, V. & Gilli, G. (1993). *Acta Cryst.* C**49**, 741–744.
Bērziņš, K., Kons, A., Grante, I., Dzabijeva, D., Nakurte, I. & Actiņš, A. (2016). *J. Pharm. Biomed. Anal.* **129**, 433–440.
Bhardwaj, R. M., McMahon, J. A., Nyman, J., Price, L. S., Konar, S., Oswald, I. D. H., Pulham, C. R., Price, S. L. & Reutzel-Edens, S. M. (2019). *J. Am. Chem. Soc.* **141**, 13887–13897.
Braun, D. E., Gelbrich, T. & Griesser, U. J. (2019). *CrystEngComm*, **21**, 5533–5545.
Braun, D. E., Nartowski, K. P., Khimyak, Y. Z., Morris, K. R., Byrn, S. R. & Griesser, U. J. (2016). *Mol. Pharm.* **13**, 1012–1029.
Case, D. H., Campbell, J. E., Bygrave, P. J. & Day, G. M. (2016). *J. Chem. Theory Comput.* **12**, 910–924.
Chisholm, J. A. & Motherwell, S. (2005). *J. Appl. Cryst.* **38**, 228–231.
Clark, S. J., Segall, M. D., Pickard, C. J., Hasnip, P. J., Probert, M. J., Refson, K. & Payne, M. C. (2005). *Z. Kristallogr.* **220**, 567–570.
Coombes, D. S., Price, S. L., Willock, D. J. & Leslie, M. (1996). *J. Phys. Chem.* **100**, 7352–7360.
Dassault Systèmes BIOVIA (2016). *Materials Studio*. San Diego, USA.
Day, G. M., Motherwell, W. D. S. & Jones, W. (2007). *Phys. Chem. Chem. Phys.* **9**, 1693–1704.
Dudek, M. K., Bujacz, G. & Potrzebowski, M. J. (2017). *CrystEngComm*, **19**, 2903–2913.
Dudek, M. K. & Day, G. M. (2019). *CrystEngComm*, **21**, 2067–2079.
Dudek, M. K., Jeziorna, A. & Potrzebowski, M. J. (2016). *CrystEngComm*, **18**, 5267–5277.
Dudek, M. K., Kaźmierski, S., Kostrzewa, M. & Potrzebowski, M. J. (2018). *Ann. Rep. NMR Spectr.* **95**, 1–81.
Dudek, M. K., Wielgus, E., Paluch, P., Śniechowska, J., Kostrzewa, M., Day, G. M., Bujacz, G. D. & Potrzebowski, M. J. (2019). *Acta Cryst.* B**75**, 803–814.
Frisch, M. J., Trucks, G. W., Schlegel, H. B., Scuseria, G. E., Robb, M. A., Cheeseman, J. R., Scalmani, G., Barone, V., Petersson, G. A., Nakatsuji, H., Caricato, M., Marenich, A. V., Bloino, J., Janesko, B. G., Gomperts, R., Mennucci, B., Hratchian, H. P., Ortiz, J. V., Izmaylov, A. F., Sonnenberg, J. L., Williams-Young, D., Ding, F., Lipparini, F., Egidi, F., Goings, J., Peng, B., Petrone, A., Henderson, T., Ranasinghe, D., Zakrzewski, V. G., Gao, J., Rega, N., Zheng, G., Liang, W., Hada, M., Ehara, M., Toyota, K., Fukuda, R., Hasegawa, J., Ishida, M., Nakajima, T., Honda, Y., Kitao, O., Nakai, H., Vreven, T., Throssell, K., Montgomery, J. A. Jr, Peralta, J. E., Ogliaro, F., Bearpark, M., Heyd, J. J., Brothers, E., Kudin, K. N., Staroverov, V. N., Keith, T. A., Kobayashi, R., Normand, J., Raghavachari, K., Rendell, A., Burant, J. C., Iyengar, S. S., Tomasi, J., Cossi, M., Millam, J. M., Klene, M., Adamo, C., Cammi, R., Ochterski, J. W., Martin, R. L., Morokuma, K., Farkas, Ö., Foresman & Fox, D. J. (2016). *Gaussian16*, Revision B.01, Gaussian, Inc., Wallingford, CT, USA.
Grimme, S., Ehrlich, S. & Goerigk, L. (2011). *J. Comput. Chem.* **32**, 1456–1465.
Grimme, S. J. (2006). *J. Comput. Chem.* **27**, 1787–1799.
Hofstetter, A., Balodis, M., Paruzzo, F. M., Widdifield, C. M., Stevanato, G., Pinon, A. C., Bygrave, P. J., Day, G. M. & Emsley, L. (2019). *J. Am. Chem. Soc.* **141**, 16624–16634.
Hofstetter, A. & Emsley, L. (2017). *J. Am. Chem. Soc.* **139**, 2573–2576.
Mackenzie, C. F., Spackman, P. R., Jayatilaka, D. & Spackman, M. A. (2017). *IUCrJ*, **4**, 575–587.
Mao, K., Wiench, W., Lin, V. S. Y. & Pruski, M. J. (2009). *J. Magn. Reson.* **196**, 92–95.
McKinnon, J. J., Jayatilaka, D. & Spackman, M. A. (2007). *Chem. Commun.* pp. 3814–3816.
Neumann, M. A. (2003). *J. Appl. Cryst.* **36**, 356–365.
Liepins, V., Skomorokhov, M., Lukjanova, N., Matiushenkov, E. & Revjuka, J. (2015). Patent No. WO 2015/181741A1.
Pettersen, E. F., Goddard, T. D., Huang, C. C., Couch, G. S., Greenblatt, D. M., Meng, E. C. & Ferrin, T. E. (2004). *J. Comput. Chem.* **25**, 1605–1612.
Piana, F., Case, D. H., Ramalhete, S. M., Pileio, G., Facciotti, M., Day, G. M., Khimyak, Y. Z., Angulo, J., Brown, R. C. D. & Gale, P. A. (2016). *Soft Matter*, **12**, 4034–4043.
Pickard, C. J. & Mauri, F. (2001). *Phys. Rev. B*, **63**, 245101.
Pienaar, E. W., Caira, M. R. & Lotter, A. P. (1993). *J. Crystallogr. Spectrosc. Res.* **23**, 785–790.
Price, S. L. (2014). *Chem. Soc. Rev.* **43**, 2098–2111.
Price, S. L. (2018). *Faraday Discuss.* **211**, 9–30.
Price, S. L., Braun, D. E. & Reutzel-Edens, S. M. (2016). *Chem. Commun.* **52**, 7065–7077.
Price, S. L., Leslie, M., Welch, G. W. A., Habgood, M., Price, L. S., Karamertzanis, P. G. & Day, G. M. (2010). *Phys. Chem. Chem. Phys.* **12**, 8478–8490.
Pulido, A., Chen, L., Kaczorowski, T., Holden, D., Little, M. A., Chong, S. Y., Slater, B. J., McMahon, D. P., Bonillo, B., Stackhouse, C. J., Stephenson, A., Kane, C. M., Clowes, R., Hasell, T., Cooper, A. I. & Day, G. M. (2017). *Nature*, **543**, 657–664.

Reilly, A. M., Cooper, R. I., Adjiman, C. S., Bhattacharya, S., Boese, A. D., Brandenburg, J. G., Bygrave, P. J., Bylsma, R., Campbell, J. E., Car, R., Case, D. H., Chadha, R., Cole, J. C., Cosburn, K., Cuppen, H. M., Curtis, F., Day, G. M., DiStasio, R. A. Jr, Dzyabchenko, A., van Eijck, B. P., Elking, D. M., van den Ende, J. A., Facelli, J. C., Ferraro, M. B., Fusti-Molnar, L., Gatsiou, C.-A., Gee, T. S., de Gelder, R., Ghiringhelli, L. M., Goto, H., Grimme, S., Guo, R., Hofmann, D. W. M., Hoja, J., Hylton, R. K., Iuzzolino, L., Jankiewicz, W., de Jong, D. T., Kendrick, J., de Klerk, N. J. J., Ko, H.-Y., Kuleshova, L. N., Li, X., Lohani, S., Leusen, F. J. J., Lund, A. M., Lv, J., Ma, Y., Marom, N., Masunov, A. E., McCabe, P., McMahon, D. P., Meekes, H., Metz, M. P., Misquitta, A. J., Mohamed, S., Monserrat, B., Needs, R. J., Neumann, M. A., Nyman, J., Obata, S., Oberhofer, H., Oganov, A. R., Orendt, A. M., Pagola, G. I., Pantelides, C. C., Pickard, C. J., Podeszwa, R., Price, L. S., Price, S. L., Pulido, A., Read, M. G., Reuter, K., Schneider, E., Schober, C., Shields, G. P., Singh, P., Sugden, I. J., Szalewicz, K., Taylor, C. R., Tkatchenko, A., Tuckerman, M. E., Vacarro, F., Vasileiadis, M., Vazquez-Mayagoitia, A., Vogt, L., Wang, Y., Watson, R. E., de Wijs, G. A., Yang, J., Zhu, Q. & Groom, C. R. (2016). *Acta Cryst.* B**72**, 439–459.

Spackman, M. A. & Jayatilaka, D. (2009). *CrystEngComm*, **11**, 19–32.

Stone, A. J. (2005). *J. Chem. Theory Comput.* **1**, 1128–1132.

TA Instruments (1998). *Thermal Solutions Software*, New Castle, DE, USA.

Thompson, H. P. G. & Day, G. M. (2014). *Chem. Sci.* **5**, 3173–3182.

Toby, B. H. & Von Dreele, R. B. (2013). *J. Appl. Cryst.* **46**, 544–549.

Turner, M. J., McKinnon, J. J., Wolff, S. K., Grimwood, D. J., Spackman, P. R., Jayatilaka, D. & Spackman, M. A. (2017). *CrystalExplorer17*, University of Western Australia.

Vinod Chandran, C., Madhu, P. K., Kurur, N. D. & Bräuniger, T. (2008). *Magn. Reson. Chem.* **46**, 943–947.

Yates, J. R., Pickard, C. J. & Mauri, F. (2007). *Phys. Rev. B*, **76**, 024401.